Primary Porcine Brain Endothelial Cells as In Vitro Model to Study Effects of Ultrasound and Microbubbles on Blood-Brain Barrier Function

S. Lélu, M. Afadzi, S. Berg, A.K.O. Åslund, S.H. Torp, W. Sattler, C. de L. Davies

Abstract— **Focused ultrasound in the presence of microbubbles transiently and reversibly opens the blood-brain barrier (BBB) in rodents and humans thereby providing a time window for increased drug delivery into brain tissue. To get insight into the underlying mechanisms that govern ultrasound-mediated opening of the BBB, in vitro models are a useful alternative. During the present study we have utilized an in vitro BBB model that consists of primary porcine brain endothelial cells (PBEC). PBEC monolayers are grown on permeable membranes, which allow assessment of key features of BBB function as well as ultrasound treatment. This experimental model is characterized by low permeability for both small molecules and proteins, has a high transendothelial electrical resistance, and expresses tight junctions and efflux pumps. Here we compare the effects of inertial and stable cavitation in presence of SonoVue microbubbles on PBEC monolayers' electrical resistance and permeability properties. Our results point out the fragility of PBEC monolayers, which enhances results variability. In particular, we show that handling of the inserts such as medium change and transfer to the ultrasound set-up modifies the cellular response, and immunostaining of the monolayers introduces damage and cell detachment within the ultrasound-exposed monolayers. Our results indicate that stable cavitation might have a more pronounced impact on cell permeability as compared to inertial cavitation in vitro. The present study might contribute to further development of experimental setups that are suitable to characterize the impact of focused ultrasound and microbubbles on BBB properties in vitro.**

Index Terms—**Blood-brain barrier, porcine brain endothelial cells, BBB model, focused ultrasound**

I. Introduction

The development of new treatment modalities targeting the central nervous system (CNS) is severely limited due to the low permeability of the vascular system forming the blood-brain barrier (BBB). The BBB ensures homeostasis and access of oxygen and nutrients to the neurons, but also prevents harmful substances and drugs to access the brain. Paracellular transport is controlled by the presence of tight and adherent junctions. A reduced number of pinocytic vesicles, an abundance of efflux pumps and highly specific transporters control transcellular transport [1]. Among the efflux pumps, P-glycoprotein or P-gp, a multidrug resistance associated protein, has been extensively studied as it can bind a broad range of substrates. Less than 2 % of the drugs developed access the brain and these drugs are small and lipophilic [2]. Transient permeabilisation of the BBB could improve treatment of brain diseases such as Alzheimer and gliomas by allowing higher amounts of drugs as well as larger and/or more hydrophilic molecules or nanoparticles to cross the BBB [3], [4]. Focused ultrasound (FUS) as a non-invasive method holds promise to enable temporary and targeted opening of the BBB, thereby allowing drug delivery to the brain. This has been demonstrated both in rats, rabbits, rhesus macaques, and recently the first clinical studies on patients with glioma were initiated [5]-[10].

A number of studies have been dedicated to obtain more knowledge on the effects of ultrasound (US) and microbubbles on BBB permeability [10], [11], and to understand the mechanisms by which US and microbubbles enhance transcytosis or open tight junctions [12]. Cavitation, i.e. formation, oscillation, and disruption of microbubbles, is

This paragraph of the first footnote will contain the date on which you submitted your paper for review. It will also contain support information, including sponsor and financial support acknowledgment. This work was supported by Helse Midt Norge.

S.L. Department of Physics, The Norwegian University of Science and technology, Høgskoleringen 5, 7491 Trondheim, Norway, sylvie.lelu@ntnu.no

M.A. Department of Physics, The Norwegian University of Science and technology, Høgskoleringen 5, 7491 Trondheim, Norway, mercy.afadzi@ntnu.no

S.B.

1: Department of Circulation and Medical Imaging, The Norwegian University of Science and Technology, Postboks 8905, 7491 Trondheim, Norway

2: SINTEF Technology and Society, Department of Medical Technology, Postboks 4760 Sluppen

7465 Trondheim, Norway, sigrid.berg@sintef.no

A.K.O.Å. Department of Physics, The Norwegian University of Science and technology, Høgskoleringen 5, 7491 Trondheim, Norway andreas.aslund@ntnu.no

S.H.T. Department of Laboratory Medicine, Children's and Women's Health, The Norwegian University of Science and Technology; Department of Pathology and Medical Genetics, St.Olavs hospital, Norway, Sverre.torp@stolav.no

W.S. Institute of Molecular Biology and Biochemistry, Medical University of Graz, wolfgang.sattler@medunigraz.at

C.deL.D. Department of Physics, The Norwegian University of Science and technology, Høgskoleringen 5, 7491 Trondheim, Norway email catharina.davies@ntnu.no

reported to be an important mechanism. Oscillation at low pressures leads to bubble oscillating for a prolonged time before it dissolves or breaks, i.e. stable cavitation. If the acoustic pressure increases sufficiently, the microbubble might collapse violently in so-called inertial cavitation. This produces a shock wave, or jet, that is strong enough to destroy tissue and penetrate cells. Consequently, it is important to tune the US exposure to find the optimal US frequency, peak negative pressure and duty cycle to obtain sufficient opening allowing nanoparticles and drugs to enter the brain tissue without causing permanent disruption of the BBB, hemorrhage, or functional damages [6], [9]. In addition, new generations of microbubbles acting as drug carriers are being developed [13]-[15]. In order to work within the safety window of the FUS exposure using various microbubbles, fine tuning of the US parameters to obtain efficient drug delivery without tissue damage has to be performed [16].

In vitro models of the BBB are valuable tools in such studies, both to reduce the number of animals used and to understand the molecular mechanisms involved during BBB opening. However, to allow valid conclusions in an in vitro BBB model, several important requirements must be fulfilled. These include low permeability, presence of developed tight junctions, expression of efflux pumps, presence of polarized receptor systems and responsiveness to cells present at the neurovascular unit [17].

Although different cell lines have been used as a BBB model, primary brain endothelial cells (PBEC) present the closest transport barrier to BBB provided their passage number is kept very low (below 3) and the cell culture pure [1]. PBEC monolayers have been shown to express trans-membrane proteins forming tight junctions such as claudins, and proteins involved in tight junctions formation such as occludin and ZO-1. They present a high resistance to the passage of ions, which is characterized by a high transendothelial electric resistance (TEER), the closest that has been reported compared to TEER estimated in vivo [18]-[21]. In addition, they express efflux proteins such as P-gp and other multidrug resistance proteins. However, the use of primary cells as in vitro BBB models is usually limited by the access to fresh and non-damaged brains.

Only a limited number of studies so far have combined the use of US and in vitro BBB models. Fan *et al.* [22] described the use of US on primary rat endothelial cells monolayers grown on permeable membranes and placed in plastic wells, but this study did not include microbubbles. Van Wamel *et al.* [23] used porcine PBEC as an in vitro model to study the effect of inertial cavitation. However, the PBEC did not form a monolayer, hence only sonoporation of single cells was studied. Kooiman et *al.* [24] used a similar set up to the one proposed here, but used HUVECs cells which do not form tight junctions [18], [19].

Here we describe some of the advantages and limitations of a BBB model based on porcine PBEC for studying the effects of US and microbubbles on junctional architecture and barrier function. It is important to be aware of the limitations and potential problems when establishing in vitro models. The PBEC model was used to study the effect of stable and inertial cavitation. A tight monolayer of PBEC was grown on a permeable insert which was placed in a sonication tank containing phosphate buffered saline (PBS) and the US transducer. The ability of the cells to form tight junctions and the effect of US on these tight junctions was investigated through TEER measurements and by immunostaining of the tight junction protein claudin 3. The effects of stable and inertial cavitation on para- and transcellular transport in porcine PBEC was investigated by studying the simultaneous transport of Lucifer yellow (LY), a very small fluorescent molecule and potential indicator of leaky tight junctions, and fluorescently labeled albumin, which is mainly transported by endocytosis.

II. Materials and methods

A. Materials

Cells culture media, antibiotics and supplements, the different solutions and enzymes used during primary cell isolation such as Medium 199, DMEM/F12, gentamicin (10 mg/mL), puromycin dihydrochloride, MEM10X (without glutamine), and dispase II, were provided by Life Technologies AS (Eugene, OR). Percoll® pH 8.5-9.5 (25°C), dextran from Leuconostoc mesenteroides used during cells' isolation, Dulbecco's phosphate buffered saline (PBS) (without calcium chloride and magnesium chloride), Penicillin/streptomycin (10,000 units penicillin and 10 mg streptomycin/mL), glutamine, fetal bovine serum (FBS), trypsin, sodium bicarbonate, Lucifer Yellow CH dilithium salt (LY), verapamil and rhodamine 123 used for characterization of P-gp, and albumin (from bovine serum), paraformaldehyde and saponin used for fixation, were purchased from Sigma Aldrich (St. Louis, MO). Corning™ Collagen I, high concentration, rat tail, was provided by Fisher Scientific (Oslo, Norway). Collagenase/dispase was purchased from Roche Applied Science (Penzberg, Germany). Collagen G was provided by Biochrom (Berlin, Germany) and goat anti-rabbit IgG H&L (Alexa Fluor® 488) and anti-claudin 3 antibody from Abcam (Cambridge, UK). Bovine Serum Albumin Alexa Fluor® 647 conjugate (BSA-AF647) was purchased from Invitrogen Molecular Probe (Eugene, OR). Cell culture inserts for multiwell plates, ThinCert™ (6 wells, 1.0 µm pore size, transparent, polyethylene terephthalate membrane) came from VWR (Radnor, PA), nylon mesh 180 µm and 60 µm from Elko Filtering Co Llc (Miami, FL), and SonoVue from Bracco SpA (Milan, Italy).

B. Isolation of porcine PBEC

Porcine brain endothelial cells (PBEC) were isolated and cultured based on a protocol originally developed by Bowman *et al.* [25] and modified by Franke *et al.*, [26]. The pig brains were collected at the local slaughterhouse. Briefly, meninges, corpus callosum, and parts of white matter were removed from the brains before mincing and enzymatic digestion of the brain hemispheres. For one brain, 70 mg of dispase in preparation medium at 37°C was added to reach a volume of 100 mL. Preparation medium consisted of Medium 199, 1 % penicillin/streptomycin, 1 % gentamicin and 1 mM glutamine.

After 90 min at 37°C, 100 mL of digested gray and white matter was mixed with 150 mL dextran solution (density=1.061) and centrifuged at 7720 g at 4°C for 10 min to collect microvessels. Microvessels were filtrated through a 180 µm nylon mesh before enzymatic digestion with collagenase/dispase II (200 µL per brain) for 1 min at 37°C to detach endothelial cells from the basement matrix. Suspended endothelial cells were collected after spinning at 1090 g for 10 min at room temperature on a Percoll gradient, re-suspended, and filtrated on a 60 µm nylon mesh before cell culturing.

C. *Culturing PBEC*

1 pig brain was used to seed 4 cell culture flasks (75 cm^2). Each flask was pre-coated with a final protein content of 0.5 mg collagen G, diluted in PBS for 1 hrs at 37°C prior to seeding. Cell growth medium consisted of Medium M199 supplemented with 10 % FBS, 1 % glutamine, 1 % penicillin/streptomycin, 1 % gentamycin, and 7 µM puromycin. The day after the isolation, cells were rinsed 3 times with PBS and growth medium was replaced. PBEC were cultured for a total of 3 days before passaging on to permeable inserts or 12 well plates, all pre-coated with collagen (120 µg collagen type I/mL ultrapure water). 1 cell culture flask was used for seeding of 6 inserts, and 4.0 x 10^5 to 5.0 x 10^5 cells were seeded per insert.

D. *Induction of tight junctions*

Cells were allowed to adhere to the permeable membrane for 48 hrs before being transferred into the cellZscope (nanoAnalytics GmbH, Münster, Germany) where growth medium was switched to induction medium. Induction medium consisted of DMEM/F12 supplemented with 1 % glutamine, 1% penicillin/streptomycin, and 550 nM hydrocortisone. The use of serum free medium and hydrocortisone is a pre-requisite to obtain the formation of tight junctions [27]. Before experiments, each insert contained on average 1.4 x 10^6 cells. Cells in the 12 well plates were grown until confluence before the growth medium was switched to induction medium.

E. *TEER measurements*

The TEER and capacitance (Ccl) of PBEC monolayers were extrapolated from the impedance spectra using cellZscope software v2.2.2 (nanoAnalytics). Cells capacitance depends on the surface of the cell membranes, with Ccl values below 1 µF/cm^2 for unfolded membranes [28]. The electrical impedance of PBEC monolayers was recorded every hour until it reached a plateau. PBEC monolayers with TEER < 200 Ω·cm^2 or Ccl>0.6 µF/cm^2 were not used for further experiments. TEER values used as references were measured less than one hour prior to US exposure. TEER ratios were calculated by dividing TEER values obtained 5 min and 24 hrs after sonication by the last TEER value measured prior to US exposure.

F. *Detection of P-gp activity by flow cytometry*

The function of P-gp on the PBEC was studied by incubating the cells with either the P-gp substrate rhodamine 123 (2.6 µM) in induction medium, or with 2.6 µM rhodamine 123 and 22.0 µM of the P-gp inhibitor verapamil. After 45-60 min at 37°C, the cells were rinsed with cold PBS. Control cells and cells incubated with rhodamine 123 were incubated with growth medium without FBS and cells incubated with rhodamine and verapamil were incubated with 10 µg/mL verapamil in growth medium without FBS for an additional 90 min at 37°C. Following incubation, the wells were rinsed with cold PBS and trypsinized. 1 mL of growth medium without FBS was added to each well and the cells were collected into flow cytometry tubes, centrifuged before being transferred into 400 µL cold PBS and stored on ice until flow cytometry analysis. The uptake of rhodamine 123 in PBEC was studied using a Gallios™ flow cytometer (Beckman Coulter Gallios, Fullerton, CA). A 488 nm laser was used for excitation and emission was detected between 505 and 545 nm. A minimum of 10000 cells were counted and the results were analyzed with Kaluza flow cytometry analysis software v1.2. Each experiment was repeated 4 times.

G. *Ultrasound set-up and exposure of the PBEC monolayers*

US signals were generated and monitored using a signal generator (33120A, Hewlett Packard, San Jose, CA), a 50 dB amplifier (ENI 2100L, Electronic navigation industries, Rochester, NY), and an oscilloscope (Waverunner, LT262, LeCroy, Chesnut Ridge, NY). A custom-made single-element 1 MHz transducer (7903A101, Imasonic SAS, Voray-sur-l'Ognon, France) with an aperture of 50 mm, and a focal distance of 12.5 cm, was used to transmit US signals in a custom-made insonication chamber (Fig. 1a). The insonication chamber was kept in a compartment maintained at 37°C. 12-24 hrs before sonication, the US chamber was filled with PBS prepared with deionized water. Deionized water was partially degassed by boiling for a minimum of 2 hrs prior to PBS preparation. The lid of the chamber was covered with a 10 mm thick sponge to prevent reflection of the sound wave. The position of the insert was easily adjusted by moving the holder supporting the insert (Fig. 1a). The membrane of the inserts was placed at 85 mm of the center of transducer, which is in the near field of the transducer. A circular area with a diameter of 15 mm in the center of the membrane received a pressure within 6 dB of the maximum pressure.

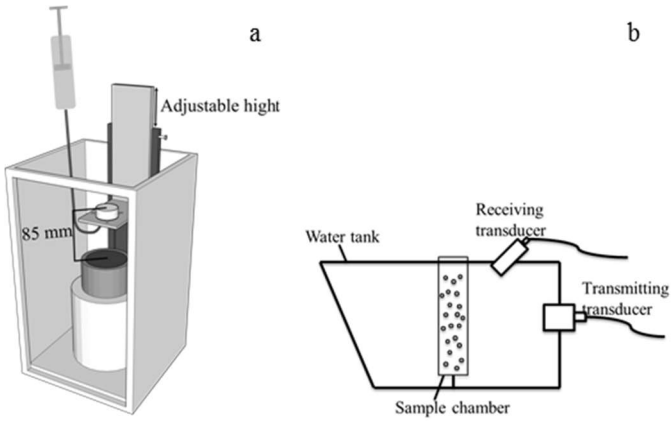

Fig. 1. Schematic representation of a: the set-up used when exposing the PBEC monolayer to ultrasound and microbubbles. The lid covered with sponge for avoiding reflection of the ultrasound waves is not shown b: the setup used for acoustic characterization of microbubbles. The incoming wave is transmitted

by the transducer mounted on the right side of the chamber and the received signal from the bubbles is picked up by the transducer mounted on the top of the chamber. The microbubbles were mixed with PBS in the sample chamber in the middle of the tank.

The insert was placed upside down in the tank with PBS. 1.4 x 10^6 cells covered the insert. The number of cells was determined by counting immunofluorescence stained cells on confocal microscopy images. SonoVue microbubbles were injected using a 1 mL syringe and a custom curved needle toward the cells (Fig. 1a). SonoVue microbubbles were re-hydrated as described by the manufacturer. An average of 280 x 10^6 bubbles/mL were counted using a light microscope and diluted to 2 % in PBS. 200 µL of diluted microbubbles was injected, which corresponded to 0.8 microbubbles per cell. Microbubbles were let to float up to the monolayer for 1 min. SonoVue microbubbles have a diameter of 2-6 µm, which is roughly similar to the dimension of PBEC. By using a ratio of 0.8/1, most of the cells should be targeted by a microbubble without the microbubbles forming a gas layer potentially interfering between the US waves and the PBEC monolayer. PBEC monolayers were either exposed to US for 60 s at a maximum mechanical index (MI) of 0.11 as a continuous wave, or for 5 s at a maximum MI of 0.8 and a duty cycle of 5 % (pulse length=50 µs and PRF=1 kHz). This corresponded to maximum peak negative pressures of 110 and 800 kPa, respectively. By applying a 60 s continuous wave and a relatively small maximum peak negative pressure (110 kPa), we expected microbubbles to oscillate continuously in the vicinity of the cells. An exposure time of 60 s was chosen to expose the BBB monolayer to microbubbles for a long time assuming that the microbubbles did not burst within 60 s at the low MI applied. When applying a maximum peak negative pressure of 800kPa on the other hand, microbubbles were expected to collapse violently within the first 5 to 10 cycles of oscillation, therefore no continuous exposure was necessary, and most bubbles should have collapsed within 5 s. Each PBEC monolayer stayed in the tank with PBS for a 4 to 5 min.

H. Acoustic characterization of microbubbles

To determine whether microbubble destruction occurs at the acoustic pressures used in this study, backscattered signals from the bubbles were captured using a separate setup as shown in Fig. 1b. Microbubble behavior could not be studied in the set up shown in Fig. 1a, as a receiver could not be inserted. Briefly, the setup consisted of a transmitting transducer (1 MHz with 85 mm focus, Ultran Group, Minneapolis, MN) placed orthogonally to the wall of a Plexiglas water tank, and a receiving transducer (5 MHz Panametrics unfocused transducer, Olympus Corporation, Tokyo, Japan) placed at an angle of approximately 45° above the transmitting transducer in the top of the tank. Prior to the experiment, SonoVue microbubbles (20.5 µl) were diluted with 60 ml of PBS in a Plexiglas chamber (width 30 mm, length 30 mm and height 80 mm) placed 60 mm from the transmitting transducer inside the water tank filled with partially degassed water. The bubbles were highly diluted to avoid bubble-bubble interaction. The transmitting transducer was driven (20 cycles with various voltages) by a 33120A Hewlett Packard signal generator and an ENI 2100L amplifier. The backscattered signal generated by the bubbles was captured by the receiving transducer, amplified (40 dB) with a pulser/receiver (5900PR Panametrics, Waltham, MA) and then recorded using the LeCroy oscilloscope at a sampling rate of 1 GSamples/s. A total of 15 bursts were recorded for each pressure level and then averaged and smoothed. The analysis of the signal was done using MatLab (Mathworks, Natick, MA). The frequency response was corrected by the frequency dependent sensitivity of the receive transducer.

I. Transport measurements across the PBEC monolayer

1.5 mL of induction medium containing 250 µM LY (Mw = 457.25 g/mol) together with 1 µM BSA-AF647 (Mw = 66.5 kDa) was added to the luminal compartment of each insert 1 to 2 min after US exposure. Two controls were included: sham immersed in the ultrasound chamber for 2 min but not exposed to US or microbubbles, and controls not placed in the PBS tank before receiving the medium with LY and BSA-AF647. Immediately upon receiving the medium containing the fluorescent tracers, the inserts were placed in a well containing 2.6 mL of fresh induction medium. The inserts were moved to a new well containing the same amount of fresh induction medium every 10 min. After 50 min the inserts were discarded and 3x50 µL aliquots were taken from each well. The fluorescence intensity of each aliquot was measured using a Tecan Infinite 200 Pro microplate reader (Tecan group Ltd, Männedorf, Switzerland). The fluorescence signal from LY was measured with a 428 nm excitation wavelength and the emission signal was recorded at 535 nm. BSA-AF647 was excited with a 650 nm wavelength and the emission signal was recorded at 701 nm. The apparent permeability (P_{app}) of the monolayers was calculated using the equation below:

$$P_{app} = \frac{1}{C_0 \cdot A} \cdot \left(\frac{dQ}{dt}\right)$$

where C_0 is the concentration of LY or BSA-AF647 at time 0, A the membrane surface area, and $\left(\frac{dQ}{dt}\right)$ the amount of fluorophore transported over time.

J. Immunofluorescence staining

PBEC monolayers were rinsed with 1 mL cold PBS and fixed on ice for 10 min with 600 µL of cold 4 % paraformaldehyde (PFA) immediately after US exposure. Then the cells were rinsed three times for 1 min with cold PBS before permeabilization with 1 mL of cold 0.05 % freshly prepared saponin. After 5 to 10 min, the saponin solution was replaced with 1 mL 1 % albumin blocking solution to minimize unspecific binding. After 30 min, 10 µg/mL anti-claudin 3 antibody diluted in 1 % albumin solution was added to each insert and incubated overnight at 4°C. Anti-claudin 3 antibody solution was then discarded, the monolayers rinsed three times with cold PBS and incubated at room temperature with 2 µL of goat anti-rabbit Alexa Fluor® 488 diluted in 1 mL PBS. After 1 hrs incubation at room temperature, the secondary antibody

was removed and the membranes were rinsed before mounting using vectashield mounting medium (Vector laboratories, Burlingame, CA). Possible nonspecific staining by the secondary antibody was imaged using a monolayer not placed in the insonication chamber, only receiving the secondary antibody.

K. *Confocal microscopy*

A SP5 Leica microscope (Leica Microsystems CMS GmbH, Mannheim, Germany) with an HPX PL APO CS 20x dry objective and a numerical aperture or 0.70 was used to image cells stained for claudin 3. Alexa Fluor® 488 was excited using a 488 nm argon laser and fluorescence detected using a hybrid detector HyD2. Image size of 512 x 512 pixels was recorded with a pinhole of 1 and 9 airy unit (AU).

L. *Data analysis*

Results were compiled and compared using SigmaPlot 13 (Systat Software, Inc. GmbH, Erkrath, Germany). Mean of the data were presented together with standard deviation, and comparison between the different treated and non-treated groups were conducted using One Way Analysis of Variance (ANOVA) test and t-test. Results were considered significant for $p<0.05$.

III. Results and Discussion

A. *Characterization of the microbubbles' behavior*

The aim of the microbubble characterization was to show the difference in behavior when applying the two different MI. The backscattered ultrasound signal from SonoVue in PBS is compared to backscattering from pure PBS and presented in Fig. 2. Strong harmonic signals from SonoVue are present with incoming pressure waves at MI=0.1. The harmonic signals are observed at multiples of the transmit frequency (2 to 9 MHz), and represent non-linear scattering, indicating that the microbubbles oscillate nonlinearly even at low MIs. Some bubbles may have been destroyed during the sonication. At MI 0.5, sub- and ultraharmonic signals appear (at 0.5, 1.5, 2.5 MHz etc.) and the noise level of the backscattered signal increases by more than 20 dB compared to MI=0.1, implying that there is a significant microbubble destruction. The bubble will expand during the negative cycle of the wave, and as the pressure increases during the positive cycle, it might collapse in a violent manner, resulting in inertial cavitation. It was not possible to generate a higher MI than 0.5 using the described 1 MHz transducer. However, the results show that even at MI=0.5 there is significant destruction, hence indicating that MI=0.8 can potentially result in inertial cavitation. Pure PBS in the sample chamber causes an increased signal at 1 MHz at both low and high MI, probably due to reflections from the chamber and possibly the presence of some air bubbles in the degassed water and in the PBS.

The shape of the frequency spectrum is increasing after 8 MHz because the recorded signal has been corrected by the frequency response of the receive transducer, which has a center frequency of 5 MHz. The shape of the noise floor is hence an inverse of the frequency response of the receive transducer.

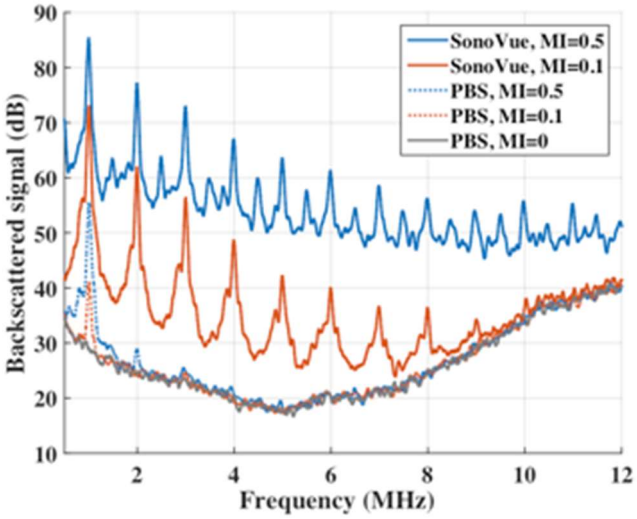

Fig. 2. Backscattering spectra of SonoVue microbubbles in PBS and from pure PBS received with a 5 MHz transducer. The signal was generated by 1 MHz transducer transmitting at different acoustic pressures with 20 cycles. A total of 15 pulses were recorded for each pressure and then averaged.

B. *Characterization of the PBEC monolayers*

Junctional architecture was characterized by immunostaining of claudin 3, a transmembrane protein involved in the formation of tight junctions. Fig. 3 shows PBEC monolayers immunostained with anti-claudin 3 after TEER values had reached a plateau (approx. 30 h after the addition of induction medium), i.e. after tight junctions were fully developed. Fig. 3a and c display a tight and homogeneous network of claudin 3, which is expressed at cellular junctions. Fig. 3a and 3b show images of the same monolayer at two different locations. On Fig. 3b, a few holes with a diameter between 10 to 100 µm are observed puncturing the monolayer, along with a few small clumps of cells on the top of the PBEC. These cell clumps are most probably cells detaching from the monolayer. The high TEER values measured prior immunostaining (Fig. 3) suggest that these cell-free areas are generated by fixation and staining. Most likely this does not occur in unstained monolayers, but it is important to be aware of these artifacts.

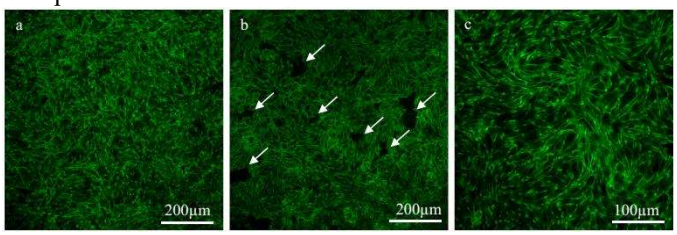

Fig. 3. Immunostaining of claudin 3 in 2 control monolayers showing the presence of tight junctions. a and b show two locations of the same monolayer. Areas free of cells are marked with an arrow. c shows a different monolayer at higher magnification. TEER values measured before immunostaining were (a and b), 417 $\Omega \cdot cm^2$, and (c), 505 $\Omega \cdot cm^2$. Ccl(a and b)=0.53µF/cm^2, and Ccl(c)=0.57µF/cm^2.

TEER measurements are a good indicator of the permeability of cell monolayers as it measures ions transport between two electrodes. In the cellZscope, the membrane supporting the PBEC monolayer was placed between the electrodes. The more restricted the paracellular transport, i.e. the more developed the tights junctions, the higher the TEER. TEER measurements were performed immediately prior to staining claudin 3, and indicated TEER values of up to 700 $\Omega \cdot cm^2$, reflecting the presence of fully developed tight junctions (Fig. 3 and 4). The low Ccl of PBEC confirms pronounced barrier properties [29]. Additionally, the TEER values determined are comparable to other primary porcine monolayers [18], [20], [30] and are much higher than in monolayers established with immortalized endothelial cell lines [20].

In order to relate the permeability of the monolayers with their TEER, the change in concentration of LY was measured and P_{app} calculated and plotted against the TEER values (Fig. 4). Higher permeability values correlated with low TEER values ($p=0.0165$) and followed an exponential decay in accordance with [31]. For TEER values above approximately 220 $\Omega \cdot cm^2$, the apparent permeability of LY stabilizes around 2.14 x 10^{-6} cm/s. These results are in agreement with in vitro models showing that minimum TEER values of 150-200 $\Omega \cdot cm^2$ represent good barrier properties [18], [19], [31].

The formation of a tight PBEC monolayer was also confirmed by comparing the permeability of LY and BSA-AF647 across empty inserts (204.0 x $10^{-7} \pm$ 39.4 x 10^{-7} cm/s and 186.0 x $10^{-7} \pm$ 58.9 x 10^{-7}cm/s for LY and BSA-AF647 respectively) and across PBEC monolayers, which were approximately 10 and 100 times smaller (LY and BSA-AF647, respectively, Fig. 7a and b).

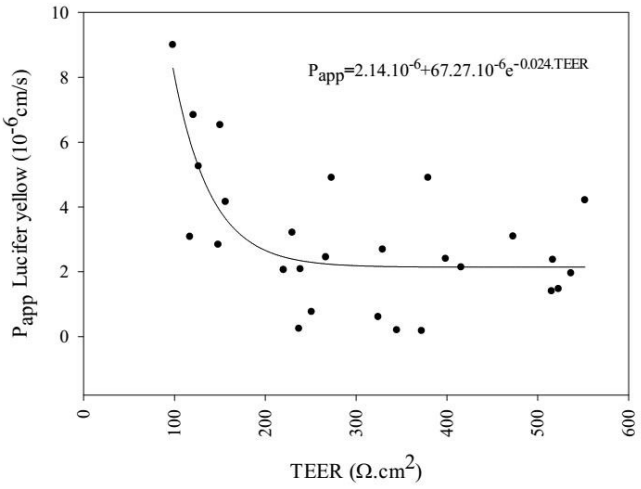

Fig. 4. The apparent permeability of LY correlated to TEER for control PBEC monolayers (R^2=0.52, p=0.0165).

One of the main features characterizing the BBB is the expression of the multidrug resistance protein P-gp. To test functionality in PBEC, rhodamine 123 (a fluorescent P-gp substrate) was added with and without verapamil (a P-gp inhibitor) to the cell medium, and the uptake of rhodamine 123 was measured by flow-cytometry. 42 % of the cells contained rhodamine 123 when no verapamil was added (Fig. 5a). The median fluorescence intensity in those cells was approximately two times higher than the autofluorescence of control PBEC, indicating that only a low concentration of rhodamine 123 remained cell-associated (Fig. 5a). The lack of complete rhodamine efflux might be due to some pumps not being efficient and/or saturation of the P-gp pumps as reported in human leukemia cell line [32]. Inhibition of the P-gp efflux pump by verapamil increased rhodamine 123 uptake up to 95 % of the cells, and the median fluorescence intensity was 14 times higher than in cells incubated with only rhodamine 123 (Fig. 5a). This demonstrates a significant increase in rhodamine 123 uptake in PBEC in the presence of the P-gp inhibitor verapamil and confirms that most of the cells do express P-gp efflux pumps.

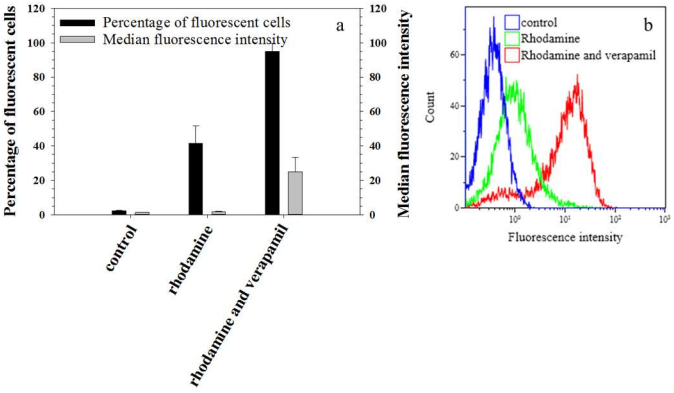

Fig. 5. P-gp is functional in PBEC. (a) Average percentage of fluorescent PBEC and median fluorescence intensity, and (b) Representative flow cytometry histogram for autofluorescence of PBEC, after incubation with rhodamine 123 alone, and after incubation with rhodamine 123 and verapamil. 7 to 10 wells were used to calculate mean values of the percentage of fluorescent cells and median fluorescence intensity.

C. Placing the monolayers in the US chamber alters TEER and permeability

Transferring the inserts into the US chamber containing PBS (sham) reduced TEER by approximately 65 %. The TEER ratios of sham-treated inserts increased two times within 24 hrs when returned to induction medium, but the TEER values did not recover completely (Fig. 6). These findings indicate that transfer of inserts into the sonication chamber severely impacts barrier function.

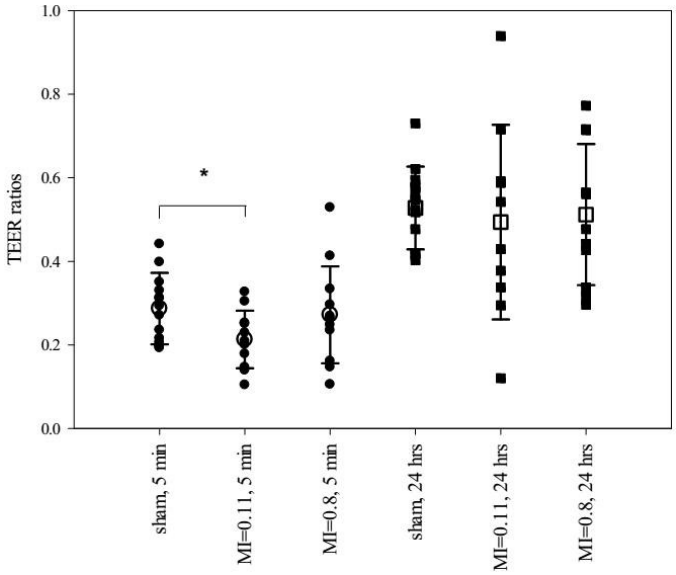

Fig. 6. TEER ratios 5 min and 24 hrs after FUS treatment. The reference measurement was taken less than 1 hrs prior to treatment. 10-14 inserts (closed symbols) were used to calculate the mean (open symbols). * indicates a significant difference from the sham.

To evaluate the role of PBS in the TEER value decrease, sham-treated inserts were placed in the tank containing DMEM/F12 at 37°C instead of PBS. Similar TEER ratio were obtained regardless whether the tank contained DMEM/F12 or PBS (data not shown), which suggests that the medium contained in the tank is not responsible for the decrease of the TEER values observed in Fig. 6.

There are, to the best of our knowledge, no studies of the effecton monolayer permeability when placing the monolayers in a tank with buffer or medium. Kooiman *et al.* [24] used a comparable set-up to the one used here with HUVEC (TEER of approximately 20 $\Omega \cdot cm^2$) cultured on permeable membranes, but TEER measurements were performed differently. An endohm-snap chamber filled with fresh medium into which the insert was transferred for TEER measurements was used; therefore the TEER value could not be compared to TEER of monolayers not moved into medium. In contrast, using the cellZcope, we compared TEER values before and after the insert had been placed into the PBS tank and moved back to the cellZcope. In another report, primary microvascular endothelial cells were isolated from rats and formed a BBB layer with TEER of approximately 180 $\Omega \cdot cm^2$. The BBB layer was exposed to US but without microbubbles [22]. The BBB model was not placed in a water tank and therefore the control group in this study cannot be compared to the sham group in Fig. 6.

The sensitivity of PBEC monolayers when placed in the tank was also reflected in the measurements of the P_{app} of both LY and BSA-AF647. The mean value of P_{app} increased significantly, by 2.3 (P_{app}(LY)=3.4 x 10^{-6} cm/s) and 3.4 (P_{app}(BSA-AF647)=6.3 x 10^{-7} cm/s), for LY and BSA-AF647 respectively, compared to controls (Fig. 7a and b). The variations between individual monolayers measurements were large.

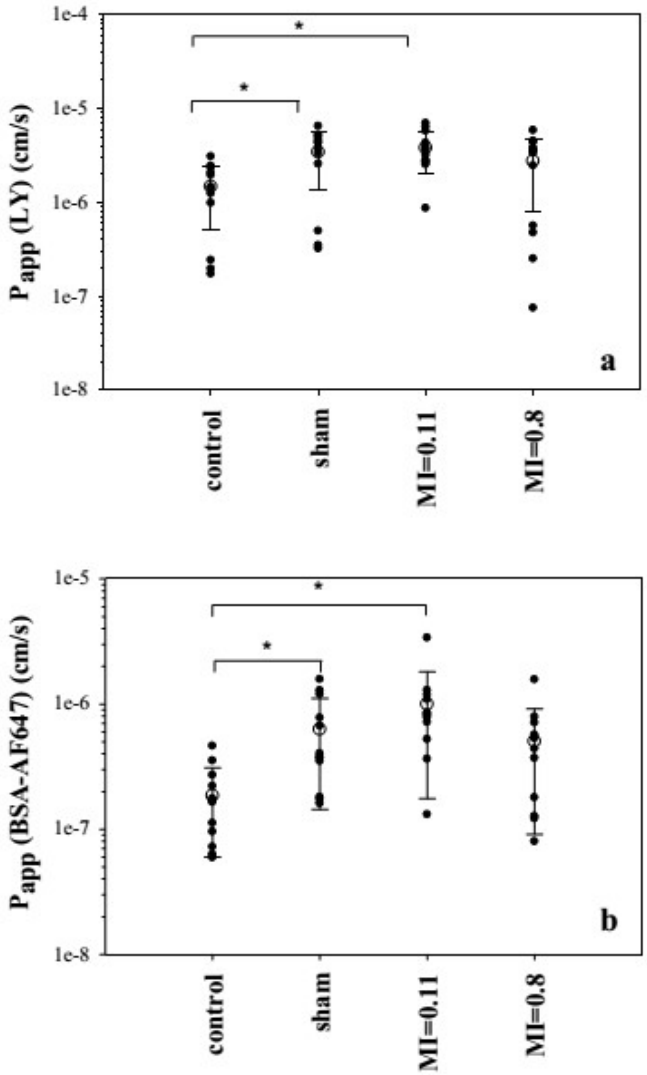

Fig. 7. Apparent permeability of LY and BSA-AF647 of control PBEC monolayers, PBEC monolayers which were placed in the sonication tank but did not received FUS (sham), and PBEC monolayers exposed to stable and inertial cavitation. Each closed circle represents one monolayer, and the open circle the mean. 12 inserts were used to calculate mean ± sd. * indicate significant differences from control.

D. Effects of US and microbubbles on the PBEC monolayers

FUS in the presence of microbubbles has been reported to open the BBB in various animal models [5], [9], [32], and acoustic pressures corresponding to an MI in the range of 0.15 to 0.80 have been used in these studies. In the present in vitro work, we compared low and high MI of respectively 0.11 and 0.80.

Fig. 6 shows the ratio of the TEER values of PBEC monolayers 5 min and 24 hrs after US exposure in the presence of microbubbles. TEER ratio tended to be reduced 5 min after applying stable cavitation, whereas inertial cavitation did not induce any significant effect. Due to large standard variations, the reduction was statistically different using t-test, but not using One Way ANOVA. No significant differences between the different groups were observed 24 hrs after exposure. As for the TEER ratios of shams, TEER ratio of PBEC monolayers exposed to US was doubled within 24 hrs when returned to

induction medium, but the TEER values did not completely recover.

The US-induced reduction of the TEER ratio was 75 % of the sham value (0.21±0.07 and 0.28±0.08 respectively), and comparable to the 60 % reduction reported by Kooiman *et al.* [24], who used a MI of 0.21 in the presence of microbubbles. Similarly, Fan *et al.* [22] reported a small reduction in the TEER value compared to untreated control, but in this study, no microbubbles were added.

The effect of US in the presence of SonoVue on P_{app} across the PBEC monolayers for LY and BSA-AF647 are shown in Fig.7a and b. US did not enhance the permeability of LY nor BSA-AF647 compared to the sham (P_{app}(sham)=3.43 x 10-6 cm/s for LY and 6.3 x 10-7 cm/s for BSA-AF647). Both sham and monolayers exposed to stable cavitation showed enhanced permeability (P_{app}(MI=0.11)=3.81 x 10-6 cm/s for LY and 10.0 x 10-7 cm/s for BSA-AF647) compared to control (P_{app}(LY)=1.47 x 10-6 cm/s and P_{app}(BSA-AF647)=1.9 x 10-7 cm/s), whereas monolayers exposed to inertial cavitation (P_{app}(LY)=2.75 x 10-6 cm/s and P_{app}(BSA-AF647)=5.0 x 10-7 cm/s) showed no significant difference (Fig. 7a and b). For BSA-AF647, the P_{app} across monolayers exposed to stable cavitation increased 1.6 times compared to sham, although the difference was not significant due to large variations. The variations between monolayers are large, especially for monolayers exposed to inertial cavitation, ranging almost over two orders of magnitude (between 0.07 x 10-6 cm/s and 5.86 x 10-6 cm/s for LY). Monolayers exposed to MI of 0.11 showed lowest variations in P_{app}. The effect of US without adding microbubbles was also measured, and the results were very similar to the sham both for TEER and permeability of LY and BSA-AF647.

The duration of the BBB opening in rats has been reported to fall within three groups: namely fast recovery within 20 s, medium closing rate within approximately 1 hrs and very slow closing of the BBB [34]. These authors also reported a correlation between vessel caliber and leakage category. It is obvious that such a categorization is not possible in in vitro systems (except isolated capillaries). It should be pointed out that in our set up, the tracer molecules were applied to the monolayer within 2 min after FUS. One report on the kinetics of pore sealing following sonoporation of single cells revealed that membrane perforation following jetting was a rapid phenomenon, with a resealing time calculated to be < 20 s [35]. The absence of effect of US on P_{app} might be due to the fact that LY and BSA-AF647 were added after resealing time. However, other reports that closing the pores takes longer time.

Immunostaining of the tight junction protein claudin 3 was in most cases very similar in controls (Fig. 8a), sham-treated inserts (data not shown), and PBEC monolayers treated with US in the presence of SonoVue (Fig. 8b and c). Bright and regular tight junctions could be seen (Fig. 8d, e, and f, higher magnification). However, the damage to the monolayers varied. Some monolayers exposed to US did not show any damage compared to the control (Fig. 8b and c), while other monolayers revealed significant cell detachment after treatment with US and SonoVue, both at MI of 0.11 and 0.8 (Fig. 8h and i). The control monolayers were either homogeneous (Fig. 8a) or presented small holes (Fig. 8g). Cell damage observed in Fig. 8h and 8i might have been aggravated by immunostaining of the inserts. The variations in US and microbubble-induced damage can explain the large variations observed in TEER values and permeability.

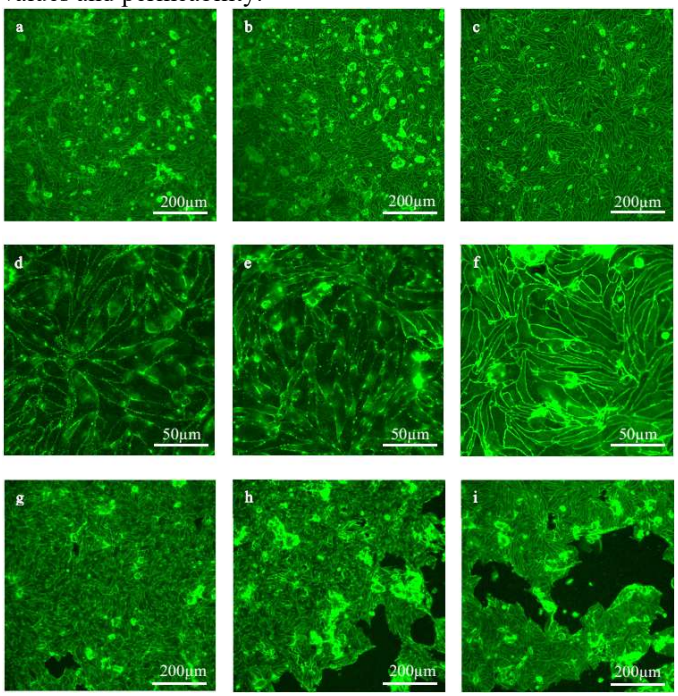

Fig. 8. Representative images of claudin 3 immunostaining of 6 PBEC monolayers. (a and g), control. (b and h), PBEC monolayers exposed to a MI of 0.11 and SonoVue. (c and i), PBEC monolayers exposed to a MI of 0.8 and SonoVue. a, b, and c show the same 3 monolayers as d, e, and f respectively, with a higher magnification. TEER measured prior to treatment ranged between 400 and 460 $\Omega.cm^2$.

LY and BSA-AF647 have been used to study paracellular and transcellular transport across monolayers, respectively [36]. However, when applying US, the tracer molecules can cross the monolayer by both routes. When cells detach from the inserts, LY and BSA-AF647 can also freely go through the pores of the membrane, and it is obvious that P_{app} does reflect neither para- nor transcellular transport.

The cell detachment observed here is probably an artifact due to cell culture condition in vitro and handling of the insert and would be unlikely to happen in vivo. In vitro, PBEC cells adhere to insert's membrane by binding to the thin layer of collagen type I coating the polyethylene terephthalate. Such binding is very fragile. In vivo, microvascular endothelial cells in the BBB are strongly interacting with each other as well as many other cell types such as astrocytes and perycites, and in addition they adhere to a complex basement matrix. In vivo, endothelial cells might be damaged as a result of exposure to ultrasound and microbubbles, but cell-cell interaction as well as the basement matrix would probably prevent detachment of the microvascular endothelial cells as observed in our model.

Additionally, our results (with the inherent limitations described and discussed above) indicate that for the PBEC model, stable cavitation was more efficient than inertial cavitation. The TEER ratio was reduced 5 min after FUS and stable cavitation also increased the apparent permeability for BSA-AF647 somewhat more than inertial cavitation. However, due to the enhanced permeability induced by placing the insert in the PBS tank, no difference was observed between the sham and stable cavitation. It should also be pointed out that there is

a large variation in the values of the P_{app}, especially when inertial cavitation was applied.

Stable and inertial cavitations affect the PBEC monolayer through different mechanisms. Stable cavitation will cause the microbubbles to oscillate, which will create fluid streaming around the bubble introducing biomechanical effects on neighboring cells. The direct effect of stable cavitation on cellular uptake and tight junction is not well understood. It is hypothesized that fluid streaming around the cell might enhance endocytosis and create cytoplasmic openings and loosen the tight junctions. A mechanical index of 0.8 will cause a rapid collapse of the microbubbles, which might result in jetting. This phenomenon has been observed in vitro to cause transient cell opening, cell depolarization, and cytomechanical perturbations [35], [37], [38], and opening of the BBB in vivo [5]-[10]. However, para- and transcellular transport should not be considered independently from each other as they have been shown to be mutually dependent [39].

The more pronounced effect of stable cavitation compared to inertial cavitation might be due to the low acoustic pressure wave pushing the microbubbles towards the BBB layer. The microbubbles thus convey direct mechanical stimuli on the monolayer for up to 60 s. Additionally, in a static in vitro model like ours, one cell is more likely to interact with the same microbubble for a longer time than in the dynamic in vivo model where new microbubbles are constantly carried by blood flow. Lastly, in our in vitro model, the high pressure wave required for inertial cavitation might have destroyed microbubbles not being in contact with the PBEC monolayer. In vivo on the other hand, endothelial cells would more likely be exposed to jetting due to the small diameter of the blood vessels.

IV. Conclusion

This study provides the first example of primary porcine brain endothelial cells used as a versatile in vitro BBB model in a functional set-up dedicated to ultrasound studies. The PBEC monolayers showed the characteristic features of a BBB model and presented restricted para- and transcellular transport. However, the results revealed the potential limitations of in vitro models, and in particular, the sensitivity and fragility of PBEC monolayers, which might results in highly variable readouts. The challenges are related to placing the monolayer into the PBS tank which reduced the TEER value and increased the permeability of the monolayer, and immunostaining of the monolayer which introduced artificial holes in control monolayers and occasionally caused detachment of large areas of cells in US-treated monolayers. Moreover, a close contact between microbubbles and cells should be ensured in vitro. This study should be useful in further establishment of in vitro models for BBB, which is highly needed to reduce the number of experimental animals and to obtain more detailed knowledge on the mechanism of US-induced opening of the BBB. However, in vitro models can never replace in vivo experiments.

Acknowledgment

The ultrasound chamber was built in Plexiglas by Finmekanisk Verksted at NTNU, Trondheim, Norway. Porcine brains were kindly provided by Sylte Gårdsslakteri AS, Surnadal, Norway, and transported by Kristin Grenstad Sæterbø.

References

[1] F. L. Cardoso, D. Brites, M. A. Brito, "Looking at the blood-brain barrier: Molecular anatomy and possible investigation approaches," *Brain Res. Rev*, vol. 64, pp. 328-363, 2010.

[2] W. M. Pardridge, "Blood-brain barrier delivery," *Drug Discovery Today*, vol. 12, pp. 54–61, Jan. 2007.

[3] B. Baseri, J. J. Choi, Y.-S. Tung, and E.E. Konofagou, "Multi-modality safety assessment of blood-brain barrier opening using focused ultrasound and definity microbubbles: A short-term study," *Ultrasound in Med. & Biol.*, vol. 36, no. 9, pp.1445-1459, 2010.

[4] F. Zhang, C.-L. Xu, C.-M.Liu, "Drug delivery strategies to enhance the permeability of the blood-brain barrier for treatment of glioma," *Drug Design, Development, and Therapy*, vol. 9, pp. 2089-2100, Apr. 2015.

[5] K. Hynynen, N. McDannold, N. Vykhodtseva , S. Raymond, R. Weissleder, F. A. Jolesz, N. A. Sheikov., "Focal disruption of the blood-brain barrier due to 260-kHz ultrasound bursts: a method for molecular imaging and targeted drug delivery," *J. Neurosurg*., vol. 105, pp. 445-454, 2006.

[6] M. Reinhard, A. Hetzel, S. Krüger, S. Kretzer, J. Talazko, S Ziyeh, J. Weber, T. Hels, "Blood-brain barrier disruption by low-frequency ultrasound," *Stroke*, vol. 37, pp. 1546-1548, 2006.

[7] F. Marquet, Y.-S. Tung, T. Teichert, V. P. Ferrera, E. E. Konofagou, "Non-invasive, transient, and selective blood-brain barrier opening in non-human primates in vivo," *PLoS ONE*, vol. 6, no. 7, Jul. 2011.

[8] X. Shang , P. Wang, Y. Liu, Z. Zhang, Y. Xue, "mechanism of low-frequency ultrasound in opening blood-tumor barrier by tight junction," *J. of Mol. Neuro*., vol. 43, pp. 364-369, 2011.

[9] N. McDannold, C. D. Arvanitis, N. Vykhodtseva, M. S. Livingstone, "Temporary disruption of the blood-brain barrier by use of ultrasound and microbubbles: Safety and efficacy evaluation in rhesus macaques," *Cancer Res*., vol. 72, no . 14, Jul. 2012.

[10] G. Samiotaki and E. E. Konofagou, "Dependence of the reversibility of focused-ultrasound-induced blood-brain barrier opening on pressure and pulse length in vivo," *IEEE Trans. on Ultrason., Ferroelect, Freq. Control.*, vol. 60, no. 11, pp. 2257-2265, Nov. 2013.

[11] J. J. Choi, K. Selert., F. Vlachos, A. Wong, and E. E. Konofagou, "Non invasive and localized neuronal delivery using short ultrasonic pulses and microbubbles," *Proc. Natl. Acad. Sci. USA*, vol. 108, no. 40, pp. 16539-16544, 2011.

[12] S. Meairs, A. Alonso, "Ultraound, microbublles, and the blood-brain barrier delivery," Prog. Biophys. Mol. Biol., vol. 93, pp. 354-362, 2007.

[13] A. K. O. Åslund, S. Berg, S. Hak, Ý. Mørch, S. H. Torp, A. Sandvig, M. Widerøe, R. Hansen, C. de L. Davies, "Nanoparticles delivery to the brain – by focused ultrasoundand self-assembled nanoparticle-stabilised microbubbles," *J. Control. Release*, vol. 220, pp. 287-294, 2015.

[14] T. Lammers, P. Koczera, S. Fokong, F. Gremse, J. Ehling, M. Vogt, A. Pich, G. Storm, M. van Zandvoort, F. Kiessling, "Theranostic USPIO-loaded microbubbles for mediating and monitoring blood-brain barrier permeation," *Adv. Func. Mater*, vol. 25, no. 1, Jan. 2015.

[15] A. van Wamel, A. Healey, P. C. Sontum, S. Kvåle, N. Bush, J. Bamber, C. de L. Davies , "Acoustic cluster therapy (ACT) - preclinical proof of principle for local delivery and enhanced uptake," *J. Control. Release*, vol. 224, pp. 158-164, 2016.

[16] K. Hynynen, "ultrasound for drug and gene delivery to the brain," *Adv. Drug Del. Rev.*, vol. 60, no. 10, pp. 1209-1217, Jun. 2008.

[17] H. C. Helms, N. J. Abbott, M. Burek, R. Cecchelli, P.-O. Couraud, M. A. Deli, C. Förster, H.-J. Galla, I. A. Romero, E. V. Shusta, M. J. Stebbins, E. Vandenhaute, B. Weksler, B. Brodin, "In vitro models of the blood-brain barrier: an overview of commonly used brain endothelial cell culture models and guidelines for their use," *J. Cereb. Blood. Flow Metab.*, Feb. 2016.

[18] A. Reichel, D. J. Begley, N. J. Abbott, "An overview of in vitro techniques for blood-brain barrier studies," in *Methods in Molecular Medicines*, vol. 89: The blood brain barrier, biology and Research protocols, S. Nag © Humana Press Inc. Totowa, NJ, 2003, pp. 307-324.

[19] M. Gumbleton, K. L. Audus, "Progress and Limitations in the use of in vitro cell cultures to serve as permeability screens for the blood-brain barrier*," J. of Pharm. Sci.*, vol. 90, no. 11, pp. 1681-1698, Nov. 2001.

[20] M. A. Deli, C. S. Ábrahám, Y. Kataoka, M. Niwa, "Permeability study on in vitro blood-brain models: Physiology, pathology, and pharmacology," *Cell. Mol. Neurobiol*., vol. 25, no. 1, pp. 59-127, 2005.

[21] A. Patabendige, R. A. Skinner, L. Morgan, N. J. Abbott, "A detailed method for preparation of a functional and and flexible blood-brain barrier model using porcine brain endothelial cells," *Brain Res*., vol. 1521, pp. 1-30, Jul. 2013.

[22] L. Fan, Y. Liu, H. Ying, Y. Xue, Z. Zhang, P. Wang, L. Liu, H. Zhang, "Increasing of blood-tumor barrier permability through paracellular pathway by low-frequency ultrasound irradiation in vitro," *J. Mol. Neurosci.*, vol. 43, pp. 541-548, 2011.

[23] A. van Wamel, A. Bouakaz, M. Versluis, N. de Jong, "Micromanipulation of endothelial cells: microbubble-cell interaction," *Ultrasound Med. Biol.*, vol. 30, no. 9, pp. 1255-1258, 2004.

[24] K. Kooiman, M. Emmer, M. Foppen-Harteveld, A. van Wamel., N. de Jong, "Increasing the endothelial layer permeability through ultrasound-activated microbubbles," *IEEE, Trans. Biomed. Eng.*, vol. 57, no. 1, Jan. 2010.

[25] F. D. Bowman, S. R. Ennis, K. E. Rarey, A. L. Betz, G. W. Goldstein, "Brain microvessels endothelial cells in tissue culture: a model for study of blood-brain barrier permeability," *Ann. Neurol.*, Vol. 14, no. 4, Oct. 1983.

[26] H. Franke, H.-J. Galla, C. T. Beuckmann, "Primary cultures of brain microvessels endothelial cells: a valid and flexible model to study drug transport through the blood-brain barrier in vitro," *Brain Res. Prot., vol. 5*, pp. 248-256, 2000.

[27] D. Hoheisel, T. Nitz, H. Franke, J. Wegener, A. Hakvoort, T. Tilling, H.-J. Galla, "Hydrocortisone reinforces the blood-brain barrier delivery in a serum free cell culture system," *Biochem. Biophys. Res. Commun.*, vol. 244, pp. 312-316, 1998.

[28] J. Wegener, D. Abrams, W. Willenbrink, H.-J. Galla, A. Janshoff, "Automated multi-well device to measure transepithelial electrical resistances under physiological conditions," *Biotechniques*, vol. 37, pp. 590-597, Oct 2004.

[29] J. Wegener, S. Zink, P. Rösen, H.-J. Galla, "Use of electrical impedance measurements to monitor β-adrenergic stimulation of bovine aortic endothelial cells," *Eur. J. Physiol*, vol. 437, pp. 925-934, 1999

[30] M. Smith, Y. Omidi, M. Gumbleton, "Primary porcine brain microvascular endothelial cells: biochemical and functional characterisation as a model for drug transport and targeting," *J. of Drug Targeting*, vol. 15, no.4, pp. 253-258, May 2007.

[31] P. J. Gaillard, A. G. de Boer, "Relationship between the permeability status of the blood-brain barrier and in vitro permeability coefficient of a drug," *Eur. J. Pharm. Sci.*, vol. 12, pp. 95-102, 2000.

[32] Y. Wang, DC. Hao, W. D. Stein, L. Yang, "A kinetic study of rhodamine-123 pumping by P-glycoprotein," *Biochim. Biophys. Acta*, vol. 1258, pp. 1671-1676, 2006.

[33] N. McDannold, N. Vykhodtseva, K. Hynynen, "Use of ultrasound pulses combined with Definity for targeted blood-brain barrier disruption: a feasibility study," *Ultrasounds in Med. & Biol.*, vol. 33, no. 4, pp. 584-590, 2007.

[34] E.E. Cho, J. Drazic, M. Ganguly, B. Stefanovic, K. Hynynen. "Two-photon fluorescence microscopy study of cerebrovascular dynamics in ultrasound-induced blood-brain barrier opening," *J. Cereb. Blood Flow Metab.*, vol. 31, pp 1852-1863, 2011.

[35] Y. Hu, J. M. F. Wan, A. C. H. Yu, "Membrane perforation and recovery dynamics in microbubble-mediated sonoporation," *Ultrasound Med. Biol.*, vol. 39, no.127, pp. 2393-2405, 2013.

[36] N. Muradashvili., R. Tyagi, D. Lominadze, "A dual-tracer method for differentiating transendothelial transport from paracellular leakage in vivo and in vitro," *Frontiers in Physiol*., vol. 3, art. 166, May 2012.

[37] P. Qin, L. Xu, Y. Hu, W. Zhong, P. Cai, L. Du, L. Jin, A. C. H. Yu, "Sonoporation-induced depolarization of plasma membrane potential : Analysis of heterogeneous impact," *Ultrasound Med. Biol*., vol. 40, no. 5, pp 979-989, 2014.

[38] Y. Hu, J. M. F. Wan, A. C. H. Yu, "Cytomechanical perturbations during low-intensity ultrasound pulsing," *Ultrasound Med. Biol.*, vol. 40, no. 7, pp. 1587-1598, 2014.

[39] W. van Driessche, J. L. Kreindler, A.B Malik, S. Margulies, S. A. Lewis, K.-J Kim, "Interrelations/crosstalk between transcellular transport functions and paracellular tight junctional properties inlung epithelial and endothelial barriers," *Am. J. Physiol. Lung Cell Mol. Physiol.* 293: L520-L524, 2007.